On the condition of streak formation in a bounded turbulent flow

K. Lam, and S. Banerjee

Citation: Physics of Fluids A: Fluid Dynamics **4**, 306 (1992);
View online: https://doi.org/10.1063/1.858306
View Table of Contents: http://aip.scitation.org/toc/pfa/4/2
Published by the American Institute of Physics

On the condition of streak formation in a bounded turbulent flow

K. Lam
Los Alamos National Laboratory, Los Alamos, New Mexico 87545

S. Banerjee
Department of Chemical and Nuclear Engineering, University of California, Santa Barbara, California 93106

(Received 14 November 1990; accepted 10 October 1991)

Flow between two surfaces at which no-slip and free-slip conditions can be imposed has been investigated numerically with a Fourier–Chebyshev pseudospectral method. Different mean shear rates have been applied to each boundary to study the effect of shear and boundary condition on the streaky structures that have been observed near walls in many previous investigations. In addition to the streaks found near the no-slip wall, the computations also reveal streaky structures when the free-slip surface is under a sufficiently high shear. The low-speed streaks observed near the free-slip surface, although appearing somewhat more pronounced, have much the same characteristics as the wall-layer streaks—e.g., the average spanwise spacing between the streaks both near the wall and the free surface is about 100 when normalized by the kinematic viscosity and the appropriate shear velocity (at the wall or at the free-slip surface). The results show that shear is much more important than the nature of the boundary in determining the dominant flow structure, rather unexpected since vortex lines can attach at a free-slip boundary whereas they cannot at a no-slip one. The formation of streaks appears to be governed by a local nondimensional shear parameter defined as $\tilde{S} \equiv S\,|\langle u'w'\rangle|/\epsilon$, where S is the mean shear rate, and $\langle u'w'\rangle$ and ϵ are the kinematic turbulent shear stress and rate of dissipation of turbulent kinetic energy, respectively. It is found that $\tilde{S} \simeq 1.0$ is the condition at which the elongated low-speed streaky regions first appear.

I. INTRODUCTION

The early experiments of Fage and Townend[1] suggested that laminar flow in its strict sense did not exist very close to the wall in a turbulent flow as hypothesized by many theories at that time. Rather, fluctuations in the spanwise velocity component were found and the flow adjacent the wall was two dimensional in planes parallel to the wall. The studies of Ferrell *et al.*[2] and Hama[3] also provided the first evidence regarding the existence of an organized structure by discovering streamwise streaks of low-speed fluid alternating in the spanwise direction in the wall region of a turbulent boundary layer. However, it is the work of a Stanford group (see, e.g., Schraub and Kline[4] and Kline *et al.*[5]), using combined dye and hydrogen-bubble visualization plus hot-wire measurements, that first systematically studied these low-speed streaks and identified their characteristics.

The low-speed streaks are generally quite regular and persistent. They have been seen in the viscous sublayer and extend into the logarithmic region. Regarding the spacing between these streaks, it has been found by many studies (e.g., Schraub and Kline,[4] Kline *et al.*,[5] Blackwelder and Eckelmann,[6] Nakagawa and Nezu,[7] Smith and Metzler,[8] and Rashidi and Banerjee[9]) that $\lambda^+ \equiv \lambda u_\tau/\nu \simeq 100$. Here λ is the average spanwise streak spacing, u_τ is the wall shear velocity defined as $\sqrt{\tau_w/\rho}$ (where τ_w = wall shear stress and ρ = fluid density), and ν is the kinematic viscosity. A number of numerical studies (e.g., Kim *et al.*[10] and Lam and Banerjee[11]) also reveal the low-speed streaks and confirm the mean spacing between them. These streaks are important because they have been observed to periodically lift off from the wall, oscillate, become unstable, break down, and lead to what are known as turbulent "bursts" (Kline *et al.*[5] and Kim *et al.*[12]). These bursts are quasiperiodic cycles of ejection of fluid away from the wall followed by an in-sweep of faster moving fluid toward the wall. The bursts have been found in various studies (e.g., Kim *et al.*,[12] Brodkey *et al.*,[13] Willmarth,[14] and Nakagawa and Nezu[15]) to account for up to 70%–80% of the production of turbulence or Reynolds stresses.

Figure 1 shows the instantaneous streamwise velocity profile associated with a wall-layer low-speed streak. (See Fig. 2 for an explanation of the coordinate system used.) The inflectional velocity profile is believed to cause the ultimate instability and breakdown of the streaks. The high-speed regions will cause fuller, more stable velocity profiles and therefore have not received as much attention as the low-speed streaks.

Despite decades of study, the origin of the low-speed streaks remains unclear. The original paper of Kline *et al.*[5] suggested that motions toward and away from the wall in the wall region would stretch and compress, respectively, the spanwise vortex elements. This stretching or compression of

 0899-8213/92/020306-15$04.00

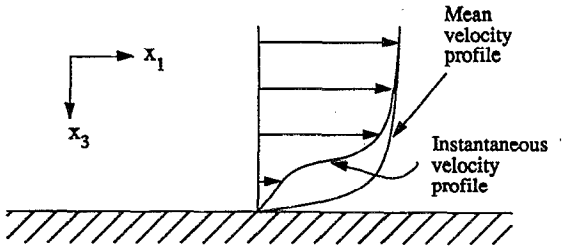

FIG. 1. Inflectional profile of instantaneous streamwise velocity profile caused by the low-speed region. The coordinate x_1 is streamwise and x_3 is normal to the wall.

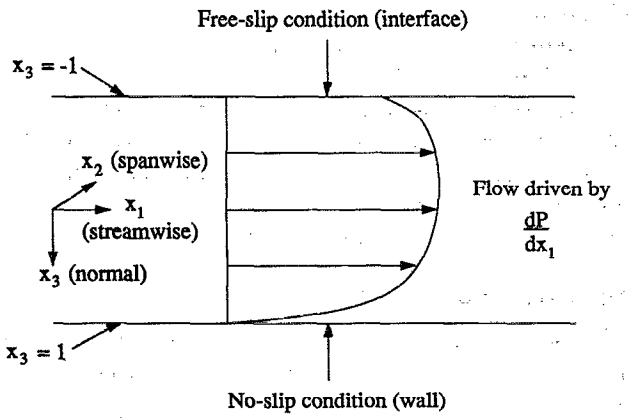

FIG. 2. Definition of problem showing the coordinate system used and the mean velocity profile. In this case, there is shear at the free surface.

vortex lines would give rise to alternating regions of high- and low-speed fluid in the spanwise direction. Unfortunately, the cause of the original inward and outward motions is still uncertain.

Some clues to the formation mechanism of the low-speed streaks are provided by the recent experiment of Rashidi and Banerjee[9] in turbulent open-channel flows. They found that low-speed streaks also occur near a sheared gas–liquid interface and their characteristics are much the same as those observed near the wall (e.g., $\lambda^+ \simeq 100$). They concluded that the shear rate has the main influence on streak formation whereas the effect of boundary conditions (no-slip at the wall and essentially free-slip at the gas–liquid interface) is much less important. This is remarkable since vortex lines can attach to a free surface, whereas they cannot at a no-slip wall. Therefore, one would expect qualitatively different behavior from the vortices near a slip surface compared to a no-slip one. The importance of shear rate in the formation of low-speed streaks has also been reported by Lee *et al.*,[16] based on comparison of results generated by numerical simulations of turbulent channel and homogeneous shear flows. These authors stated that high shear rate alone is sufficient for generation of the low-speed streaks and the presence of a solid boundary is not necessary. They proposed that a local nondimensional group which controls streak formation might be given by $S^* \equiv Sq^2/\epsilon$, where S is the shear rate, q^2 and ϵ are, respectively, twice the turbulent kinetic energy per unit mass and its rate of dissipation. However, results in Rashidi and Banerjee[9] suggested that S^* might not be the correct structural parameter in flows with a gas–liquid interface. This is because the interface ϵ becomes rather small but q^2 does not due to motions parallel to the interface.

To clarify the physical conditions that control streak formation the present study further investigates streaky structures occurring near no-slip and free-slip surfaces. The shear rates at a no-slip wall and at a free-slip surface have been varied systematically in a series of numerical simulations. The effect of shear on the streaky structures near both the wall and the free-slip surface were examined. The goal is to determine whether a suitable parameter can be found to express the critical condition (combination of shear rate and turbulence properties of the flow) that governs the formation of streaks. This is of course only one objective of the numerical simulations. Later reports will deal with the behavior of quasistreamwise vortices which are seen near the boundaries at sufficiently high shear rates and appear to be associated with ejection–in-sweep cycles. These vortices are of smaller streamwise length than the low-speed streaks.

II. NUMERICAL SIMULATION OF FLOW BETWEEN A FREE-SLIP SURFACE AND A NO-SLIP WALL

The problem considered is an incompressible flow driven by a pressure gradient (or gravity) between a wall under the no-slip condition and a surface under the free-slip condition, as shown in Fig. 2. The coordinates x_1, x_2, and x_3 are used to represent, respectively, the streamwise, spanwise, and normal directions. By the free-slip condition, we mean that the velocity fluctuations parallel to the surface are not restrained and obey boundary conditions to be given below. In our simulations, the free-slip surface is under no shear in one case or there can be a constant mean shear imposed in other cases. A close physical analog of this problem is the flow of a liquid stream with or without counter-current gas flow above it, such as the flow studied in the experiments of Rashidi and Banerjee.[9,17] The boundary condition on the liquid side at the gas–liquid interface is essentially free-slip because velocity fluctuations parallel to the interface are unimpeded (unlike at the wall) due to the much lower density (hence, inertia) of the gas. The condition of a flat interface (i.e., with negligible surface waves) could be achieved in the experiments by keeping the Froude number and the relative velocity between the liquid and the gas low to avoid surface instabilities.

The full time-dependent Navier–Stokes equation for the flow considered were integrated numerically starting from some artificial initial conditions. After statistically steady solutions had been attained, the integration was continued for some additional time steps to allow for storage of a time record of velocity fields. Then these velocity fields could be used to obtain turbulence statistics and as data for conditional sampling and simulation of flow visualization experiments. This approach to investigating turbulence via direct numerical simulation has become practical due to the advent of high-speed and large-memory supercomputers. Recent

applications of such an approach include Gerz *et al.*[18] on stratified turbulent flows in water and in air, Kim *et al.*[10] on fully developed channel flow, Rogers and Moin[19] on homogeneous shear flows, and Riley *et al.*[20] on mixing layers with chemical reactions. General reviews on numerical simulation of turbulence are given by Schumann *et al.*[21] and Rogallo and Moin.[22] In the following, we shall briefly describe the numerical procedures used in our study.

A. Numerical procedures

The basic governing equations are the mass and momentum conservation equations for an incompressible, Newtonian fluid:

$$\frac{\partial u_j}{\partial x_j} = 0, \tag{1}$$

$$\frac{\partial u_i}{\partial t} = S_i + \frac{1}{\mathrm{Re}}\nabla^2 u_i - \frac{\partial p}{\partial x_i}, \tag{2}$$

where u_i are the velocity components, $\partial p/\partial x_i$ are the kinematic pressure (pressure divided by the mass density) gradients minus the mean part, and S_i are the nonlinear convective terms minus the mean kinematic pressure gradient. All variables are normalized by half of the liquid depth h and the effective shear velocity defined as

$$u_{*e} \equiv \sqrt{h\Pi}, \tag{3}$$

where Π is the magnitude of the mean kinematic pressure gradient that drives the flow. This definition of the shear velocity is desirable for the cases where shear rates are present at both boundaries. The Reynolds number Re is defined as $u_{*e}h/\nu$, where ν is the kinematic viscosity. The pressure gradients $\partial p/\partial x_i$ can be eliminated to give the following set of equivalent equations:

$$\frac{\partial \omega_k}{\partial t} = \epsilon_{ijk}\frac{\partial S_j}{\partial x_i} + \frac{1}{\mathrm{Re}}\nabla^2\omega_k, \tag{4}$$

where $\omega_k = \epsilon_{ijk}(\partial u_j/\partial x_i)$ is the vorticity, and

$$\frac{\partial}{\partial t}(\nabla^2 u_i) = \nabla^2 S_i - \frac{\partial}{\partial x_i}\left(\frac{\partial S_j}{\partial x_j}\right) + \frac{1}{\mathrm{Re}}\nabla^4 u_i. \tag{5}$$

Equations (4) and (5) are then written for the normal component, i.e., for ω_3 and u_3, respectively:

$$\frac{\partial \omega_3}{\partial t} = \frac{\partial S_2}{\partial x_1} - \frac{\partial S_1}{\partial x_2} + \frac{1}{\mathrm{Re}}\nabla^2\omega_3, \tag{6}$$

$$\frac{\partial}{\partial t}(\nabla^2 u_3) = \nabla^2 S_3 - \frac{\partial}{\partial x_3}\left(\frac{\partial S_j}{\partial x_j}\right) + \frac{1}{\mathrm{Re}}\nabla^4 u_3. \tag{7}$$

These two equations will be solved for u_3 and ω_3 with the numerical method outlined below. With u_3 and ω_3 known, u_1 and u_2 can be obtained by solving the following simultaneously:

$$\frac{\partial u_1}{\partial x_1} + \frac{\partial u_2}{\partial x_2} = -\frac{\partial u_3}{\partial x_3} \quad \text{(continuity)}, \tag{8}$$

$$\frac{\partial u_2}{\partial x_1} - \frac{\partial u_1}{\partial x_2} = \omega_3 \quad \text{(definition of vorticity)}. \tag{9}$$

Although not needed for time advancement (see below) of the solutions, the pressure can be obtained, say, for turbulence statistics, by solving a Poisson-type equation after all the velocity components have been found.

The solution method is similar to that used by Kim *et al.*[10] in their simulation of turbulent channel flow. Therefore, the reader is referred to that paper and Lam[23] for the derivations and details. While the methodology is similar to that of Kim *et al.*, the computer code was developed independently and undoubtedly differs in many details. For this reason, the results of some checks are provided in this paper, in Lam,[23] and in Lam and Banerjee.[11] Only a synopsis of the method and some important equations are given here.

Time advancements of Eqs. (6) and (7) is done by the two-level explicit Adams–Bashforth scheme for the convective S_i terms and by the implicit Crank–Nicolson method for the diffusion terms. The solutions in space are represented by Fourier expansions with N_1 and N_2 terms, respectively, in the homogeneous directions x_1 and x_2, and by N_3 Chebyshev polynomials in the normal (x_3) direction. After the Fourier transform of Eqs. (6)–(9) is taken, a set of differential equations in x_3 for the Fourier coefficients at each wave-number pair (k_1,k_2) can be written. At the wall ($x_3 = 1$) the usual no-slip boundary conditions are applied:

$$\hat{u}_1 = \hat{u}_2 = \hat{u}_3 = 0, \tag{10}$$

where $\hat{u}_1$, $\hat{u}_2$, and $\hat{u}_3$ are Fourier transforms (or coefficients) of the velocity components. At the free-slip surface ($x_3 = -1$), the boundary conditions are

$$\hat{u}_3 = 0, \tag{11}$$

$$\frac{\partial \hat{u}_1}{\partial x_3} = \frac{\partial \hat{u}_2}{\partial x_3} = 0. \tag{12}$$

Equation (11) expresses the condition that fluid motions normal to the surface are damped by surface tension, if a gas–liquid interface is considered. The free-slip conditions as given by Eq. (12) imply that the fluid is "free" to fluctuate parallel to the surface. Boundary conditions (10)–(12) are applied to $\hat{u}_i$ for all wave numbers (k_1,k_2) for the case of no interfacial shear. The Fourier coefficients at $k_1 = k_2 = 0$ represent the solutions averaged over the homogeneous directions (i.e., over the x_1-x_2 plane). Therefore, we can simulate the average effect of a counter-current gas flow with the following boundary condition for $\hat{u}_1$ at $k_1 = k_2 = 0$:

$$\hat{u}_1 = (1/N_1N_2)U_0 \quad \text{at } x_3 = -1, \tag{13}$$

where U_0 is the average interfacial velocity normalized by u_{*e}. As the counter-current gas flow is increased, U_0 will decrease, hence increasing the shear at the interface (see Fig. 3 in the next section). Therefore cases where there is a different shear at the interface can be simulated by specifying different values for U_0.

Because Eq. (7) is fourth order in u_3, two additional boundary conditions are required. In terms of the Fourier transforms, these are

$$\frac{\partial \hat{u}_3}{\partial x_3} = 0 \quad \text{at } x_3 = 1, \tag{14}$$

$$\frac{\partial^2 \hat{u}_3}{\partial x_3^2} = 0 \quad \text{at } x_3 = -1. \tag{15}$$

Equations (14) and (15) are obtained from applying the continuity equation at the wall and its derivative in x_3 at the free-slip surface, respectively.

B. Computational runs

The first case we studied was one with no shear at the interface. (The surface $x_3 = -1$ will be referred to interchangeably as the interface, the free surface, or the free-slip surface.) The Reynolds number Re is 60.4, based on the half-depth h and the effective shear velocity u_{*e} defined in Eq. (3). (Note that h is the half-depth in this expression so that u_{*e} differs by a factor of $\sqrt{2}$ compared to the wall shear velocity for the case with an unsheared free surface.) The corresponding Reynolds number Re_D, based on average velocity and equivalent diameter, is 11 000 and Re_τ, based on wall shear velocity u_τ and total depth, is 171. The particular Reynolds number was chosen because experimental data (wall-bounded channel flow of Kreplin and Eckelmann,[24] $\mathrm{Re}_\tau = 194$; open channel flows of Komori *et al.*,[25] $\mathrm{Re}_D = 11\,000$, and of Rashidi and Banerjee,[17] $\mathrm{Re}_D \simeq 14\,000$–$60\,000$) are available for comparison with some of the statistics obtained from the simulation. In addition, turbulence statistics in fully developed channel flow, between parallel plates, at $\mathrm{Re}_\tau = 180$ have been obtained by Kim *et al.*[10]

While the results reported here and those of Kim *et al.*[10] can be expected to be similar near what is the "no-slip" boundary in our case—provided the shear rates are high enough—they will differ as we get closer to our free-slip surface. Even in the case where the shear rate is zero at the free-slip surface, our case does not reduce to that of Kim *et al.* in the region of the centerplane of their channel flow. The reason is obvious, viz., only the wall-normal component of the vorticity can exist at our free-slip surface which corresponds to the centerplane of the Kim *et al.* simulations, where the vorticity vector can have arbitrary orientation.

The relatively low Reynolds number chosen is a practical limitation of direct numerical simulation of turbulence in general. This is because the ratio between the largest and the smallest (dissipative) scales of motion grows as $\mathrm{Re}_D^{9/4}$ when all three dimensions are considered. However, as pointed out in Rogallo and Moin,[22] the attraction of direct turbulence simulation is that it eliminates the need for *ad hoc* models, and the justification often given is that the statistics of the large scale vary little with Reynolds number and can be found at the low Reynolds numbers required for full simulation.

The size of the computational domain, $L_1 \times L_2 \times L_3$, is $4\pi h \times 2\pi h \times 2h$. The selection of the periodicity lengths L_1 and L_2 was guided by the two-point correlation measurements of Comte-Bellot[26] and the numerical simulations of Moin and Kim[27] and Kim *et al.*[10] for channels flows. Both the experimental data and computations (including the present study) showed that the correlation between velocity fluctuations at two points became negligible beyond a streamwise separation of $\sim 3.2h$ and a spanwise separation of $\sim 1.6h$. Therefore, we believe that the above values of L_1 and L_2 were large enough to justify the periodicity assumptions implied by the Fourier representation of the solutions in the x_1 and x_2 directions. Another requirement on the size of the computational domain was that it must contain several of the wall-layer streaks which are the focus of this study. In wall units, $L_1^+ \times L_2^+ \times L_3^+$ is $1073 \times 537 \times 171$. Therefore, based on the mean spanwise streak spacing $\lambda^+ \simeq 100$, at least several streaks would be covered in the solution domain.

In the simulation, 32 and 64 Fourier modes in x_1 and x_2, respectively, and 65 Chebyshev polynomials in x_3 were used to represent the solutions. The corresponding grid resolution in wall units is $\Delta x_1^+ = 33$, $\Delta x_2^+ = 8.4$, and Δx_3^+ is 0.1 next to the wall or interface ($x_3 = \pm 1$) but increases to 4.2 near the center of the flow ($x_3 = 0$). The estimated Kolmogorov scale at around 15 wall units from the wall, $\eta^+ \equiv \eta u_\tau / \nu$, where $\eta = (\nu^3/\epsilon)^{1/4}$, is about 2, which is smaller than the resolution of the computation in the streamwise and spanwise directions. However, the computed results, when compared with available experimental data (see next section), indicated that the unresolved dissipative scales did not seem to cause serious errors. This problem of not resolving the smallest scales of motion was also encountered and discussed in Kim *et al.*[10] They noted that the significant dynamic roles, if any, of the neglected small or dissipative eddies would only be clarified by numerical experiments with much finer resolution, which are very time consuming and difficult to do on today's computers. However, comparison of their numerical results with those obtained with a somewhat coarser resolution revealed no differences in the statistical correlations they considered.

The calculations were started with initial conditions that consisted of the mean profiles for u_1 (the universal wall profile), u_2 and u_3 (both are zero throughout the liquid layer) superimposed with sinusoidal perturbations in all three dimensions. The initial perturbations contained the first odd and even modes. Higher-order modes were generated as the governing equations were integrated in time through nonlinear interactions. The time step size Δt used was chosen for each run such that a limit defined as

$$\left|\frac{u_1 \Delta t}{\Delta x_1}\right| + \left|\frac{u_2 \Delta t}{\Delta x_2}\right| + \left|\frac{u_3 \Delta t}{\Delta x_3}\right| < 0.3$$

was satisfied everywhere in the flow. This limit was empirically determined and not based on theoretical analysis. In practice, throughout all the computations, the limit was more usually around 0.2, and was dominated by $|u_3 \Delta t / \Delta x_3|$ because of the fine Chebyshev resolution, Δx_3, near the flow boundaries.

We have also studied cases in which the interface is under shear. The amount of shear imposed depends on the specified value of the average interfacial velocity (normalized by u_{*e}), U_0 as discussed in the previous section. Figure 3 shows the computed mean velocity profiles of three cases with different shear at the interface, in addition to that of the first run with no interfacial shear. Table I lists the values of U_0 and quantities related to shear stresses for seven runs we have performed (see the next section for definition of various quantities).

The runs with interfacial shear (cases II–VII) were done at a slightly higher Reynolds number, $\mathrm{Re} = 85.4$, because there is flow resistance at the interface, in addition to the wall. The number of modes and the computational domain size were the same as those used in the case with no

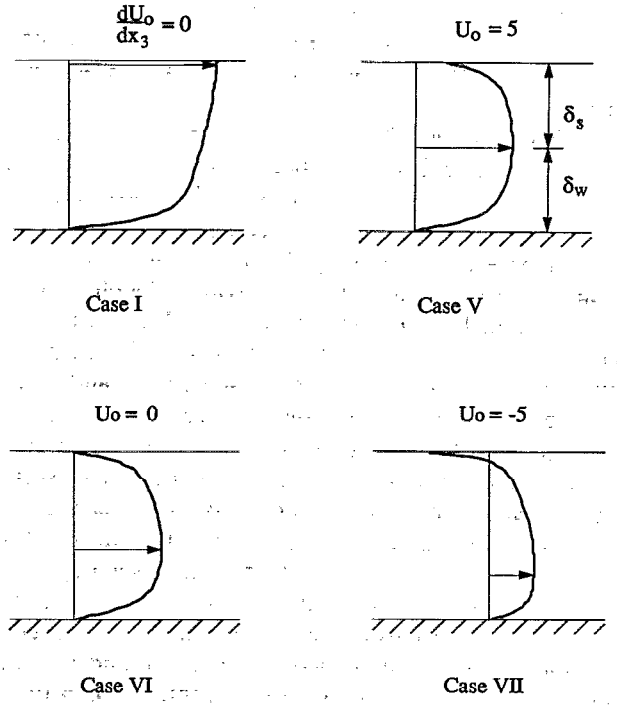

FIG. 3. Computed mean velocity profiles for several cases studied. Note changes in the location of maximum velocity and in the velocity gradient at both the wall and the free surface as the average interfacial velocity U_0 is varied.

interfacial shear. The initial conditions for each run were obtained from the solutions of a performed run which has a similar mean velocity profile. For example, the calculations for case II were started with the solutions of case I at a particular instant of time.

The computer memory required for the computations (with the present resolution) was around two million 64-bit words. The calculations took 1.5 CPU and system seconds per time step on a Cray X-MP/48 computer. The total amount of computer time used (for integration plus subsequent analysis) was about 100 h, a significant portion of which was spent on calculations involving turbulence statistics, flow visualization, etc.

III. RESULTS AND DISCUSSION

In case I, the solutions became statistically steady, starting from the imposed initial conditions, after a time of about $6h/u_{*e}$. The other cases reached statistically steady state a little sooner—after a time of about $4h/u_{*e}$. This is because each of the latter runs was started with the solutions of a run under slightly different interfacial shear. After equilibrium had been reached, velocity fields at about 600 time intervals spanning $4h/u_{*e}$ were stored for post-processing.

TABLE I. Run parameters for all the cases studied.

Run case	I	II	III	IV	V	VI	VII
U_0 (b.c.)		18	15	10	5	0	−5
u_{*s}^2/u_{*e}^2	0.0	1.8	1.5	1.4	1.0	0.7	0.5
u_{*w}^2/u_{*e}^2	2.0	0.2	0.5	0.6	1.0	1.3	1.5
Re_{*s}	0	7.6	26	37	85	122	168
Re_{*w}	171	206	164	146	85	53	28

An indication of the solutions becoming statistically steady (at least up to the second moments) could be given by the shear stress profile. For the fully developed flows in this study, the equilibrium profile of the total shear stress τ is linear in x_3:

$$\tau/\rho u_{*e}^2 = (\tau_s/\rho u_{*e}^2) + (x_3 + 1), \tag{16}$$

where τ_s is the shear stress at the interface, $x_3 = -1$.

The shear stress at the wall, τ_w, can be obtained from Eq. (16) as

$$\tau_w/\rho u_{*e}^2 = (\tau_s/\rho u_{*e}^2) + 2. \tag{17}$$

Defining shear velocities at the wall and at the interface as $u_{*w}^2 \equiv |\tau_w|/\rho$ and $u_{*s}^2 \equiv |\tau_s|/\rho$, and noting that τ_w and τ_s have opposite signs, we can write

$$u_{*w}^2 + u_{*s}^2 = 2u_{*e}^2. \tag{18}$$

From case II to case VII, the interfacial shear velocity u_{*s} was increased and, because u_{*e} (proportional to Re) is constant in those runs, u_{*w} was decreased. Table I lists the values of these shear velocities for all the runs. Also listed are values of the local shear Reynolds numbers, Re_{*s} and Re_{*w}, defined as

$$\mathrm{Re}_{*s} \equiv u_{*s}\delta_s/\nu, \tag{19}$$

$$\mathrm{Re}_{*w} \equiv u_{*w}\delta_w/\nu, \tag{20}$$

where δ_s and δ_w are, respectively, the distances from the interface and from the wall to the location of maximum velocity (see Fig. 3). We shall use Re_{*s} and Re_{*w} as a measure of the amount of shear imposed at the interface and at the wall, respectively.

Figure 4 shows the profiles of $\tau/\rho u_{*e}^2$ for cases I and V. The total shear stress was calculated from the following relation:

$$\frac{\tau}{\rho u_{*e}^2} = \frac{1}{\mathrm{Re}}\frac{d\langle u_1\rangle}{dx_3} - \langle u_1' u_3'\rangle, \tag{21}$$

where $\langle\ \rangle$ denotes averaging in time and in the homogeneous (x_1 and x_2) directions and the prime indicates fluctuations from the mean. Note that the total stress profiles are linear as expected and that in case V the shear at the interface was about the same as that at the wall.

In the following subsection we shall compare some of the computed turbulence statistics with available data. Results from case I have been chosen. The purpose there is to verify the accuracy of the numerical method. Results related to the low-speed streaks and various local shear related quantities important for streak formation will be presented in subsections B and C.

A. Comparison of turbulence statistics with previous work

In this section, the computed turbulence statistics for case I are compared with previous studies. The mean velocity profile, turbulence intensities, and skewness and flatness

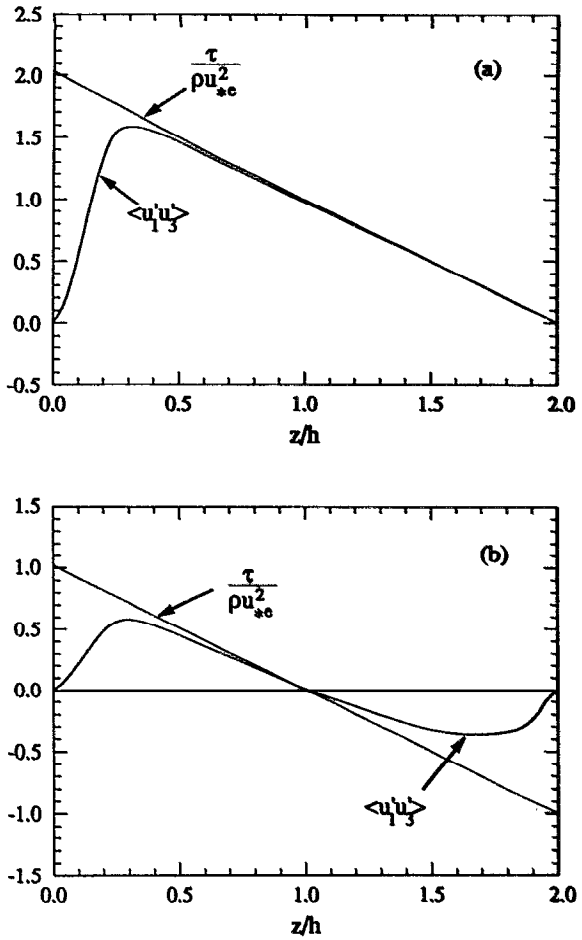

FIG. 4. Profiles of the computed total shear stress τ, normalized by ρu_{*e}^2, and the nondimensional Reynolds stress $\langle u_1' u_3' \rangle$ for (a) case I and (b) case V.

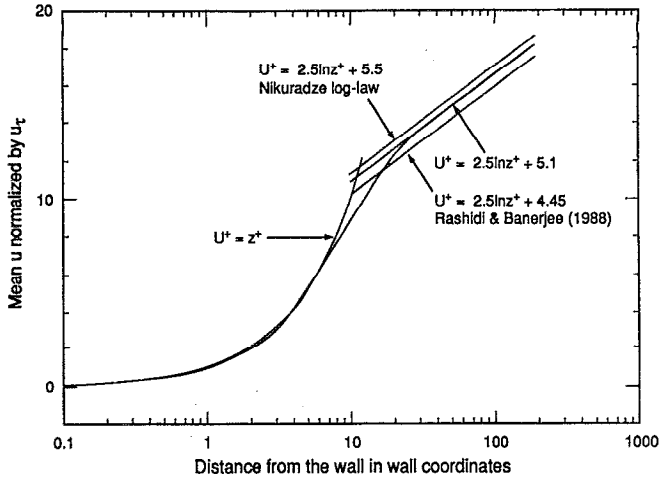

FIG. 5. Comparison between the computed and experimental mean velocity profiles in case I. The normalized mean velocity U^+ is plotted against $z^+ \equiv z u_\tau / \nu$.

factors will be discussed. More statistics (e.g., pressure fluctuations, turbulence kinetic energy balance terms) can be found in Lam.[23] In the following, the velocity components (u,v,w) are the dimensional counterparts of (u_1,u_2,u_3). In place of (x_1,x_2,x_3), the dimensional coordinates (x,y,z) are used, with z representing distance from the wall.

Figure 5 shows the profile of the computed mean velocity normalized by the wall shear velocity ($U^+ = U/u_\tau$). Within the viscous sublayer ($z^+ < 5$ where $z^+ = z u_\tau/\nu$), the expected linear law of the wall $U^+ = z^+$ is followed. In the logarithmic region ($z^+ > 30$), the calculated mean velocity behaves as

$$U^+ = 2.5 \ln z^+ + 5.1. \tag{22}$$

For comparison, the common Nikuradze logarithmic law

$$U^+ = 2.5 \ln z^+ + 5.5 \tag{23}$$

for turbulent boundary layers and the profile reported in Rashidi and Banerjee,[17]

$$U^+ = 2.5 \ln z^+ + 4.45, \tag{24}$$

for open-channel flows are also plotted. The low value of the constant in Eq. (24) is probably due to some wall roughness in the Rashidi and Banerjee experiment, as they pointed out themselves. However, the constant in the calculations [Eq. (22)] being lower than 5.5 in the Nikuradze profile [Eq. (23)] requires discussion. An extensive and careful study of velocity profiles by Nezu and Rodi[28] revealed that there were systematic differences between the constants in open-channel flow compared to boundary layers and closed channel flows. They noted that for $z^+ > 30$ but $z/h < 0.2$

$$U^+ = 2.43 \ln z^+ + 5.29. \tag{25a}$$

However, if the region was extended to $z^+ > 30$ but $z/h < 0.6$ the velocity profile was fitted by

$$U^+ = 2.5 \ln z^+ + 4.76. \tag{25b}$$

They concluded that the second constant in Eq. (25b) is considerably smaller than 5.5 if the first constant is 2.5. This is in line with our direct simulations. The reasons are not clear at present, but probably have to do with the difference in Reynolds stress profiles required by the free-surface

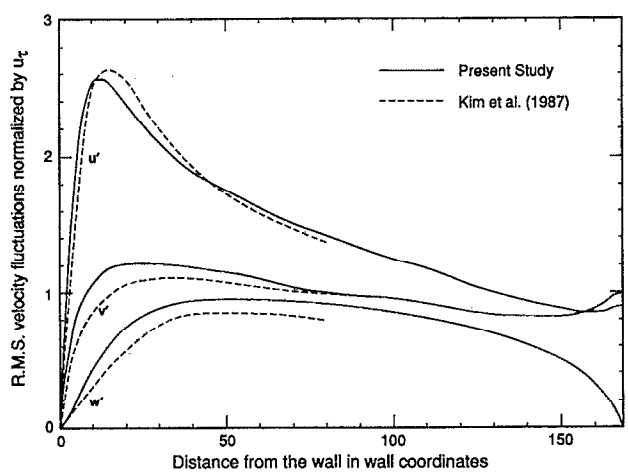

FIG. 6. Comparison between the computed rms velocity fluctuations in case I with the numerical channel flow data of Kim *et al.* (Ref. 10) $u_{\rm rms} \equiv \sqrt{\langle u'^2 \rangle}$, $v_{\rm rms} \equiv \sqrt{\langle v'^2 \rangle}$, $w_{\rm rms} \equiv \sqrt{\langle w'^2 \rangle}$.

boundary condition. In the computed profile, the small deviation from the log profile near the surface (i.e., a Cole's wake region) as found in Nezu and Rodi is not seen. This is because the deviations are significant only for high Reynolds numbers ($Re_D \geqslant 55\,000$).

Figure 6 shows the computed root-mean-square (rms) velocity fluctuations u_{rms}, v_{rms}, and w_{rms} normalized by u_τ. The results agree reasonably well with the near-wall channel flow data (not shown in Fig. 6) of Kreplin and Eckelmann.[24] However, the numerical data of Kim *et al.*[10] have been widely accepted; therefore, the computed near-wall rms velocity fluctuations from that study are plotted in Fig. 6 for comparison. The agreement in the shape of the profiles is quite good. However, the spanwise and normal fluctuations are somewhat higher than those in Kim *et al.*

For comparison with data close to the interface, the computed rms profiles are shown in Fig. 7, together with those measured by Komori *et al.*[25] and Rashidi and Banerjee.[17] Data for u_{rms} and w_{rms} at $Re_D \simeq 14\,000$ of Rashidi and Banerjee and for u_{rms}, v_{rms}, and w_{rms} at $Re_D = 11\,000$ of Komori *et al.* are plotted. The computed u_{rms} and v_{rms} are enhanced while w_{rms} is damped as the free surface is approached, in agreement with the experimental data. This behavior can be explained as the redistribution of the normal turbulent kinetic energy $\frac{1}{2}w_{rms}^2$ into the streamwise and spanwise components $\frac{1}{2}u_{rms}^2$ and $\frac{1}{2}v_{rms}^2$ through the pressure–strain correlation terms in the turbulent kinetic energy transport equations (see Lam and Banerjee[11]).

As shown in Fig. 7, the computed rms values agree fairly well with the experimental results. Note that the discrepancy between the two sets of experimental data is in general larger than the deviation of the present results from either experiment. A possible cause of the discrepancies between the computed and the experimental results is the uncertainty in the normalizing factor u_τ, which was not measured directly in the experiments. Rather, the wall shear velocity u_τ was deduced from the measured mean velocity profile and use of either a logarithmic formula or the Blasius equation. Finally, the experimental values of w_{rms} did not vanish at the interface. This was probably due to the slight waves present in the experiments.

The computed skewness factors for the velocity fluctuations u', v', and w' are shown in Fig. 8. As pointed out in Kim *et al.*,[10] the skewness factor of the spanwise fluctuations $S(v')$ should be zero everywhere because of the reflection symmetry of the solutions of the Navier–Stokes equations. The deviation of the computed $S(v')$ from zero as shown in Fig. 8 indicates that the sample size used for statistical averaging of the numerical results is at best marginal for these high-order statistics. Nevertheless, $S(u')$ and $S(w')$ near the wall agree roughly with the numerical data (not shown in Fig. 8) of Kim *et al.*[10] The experimental data of Nakagawa and Nezu[15] for $S(u')$ and $S(w')$ in an open-channel flow ($Re_D = 44\,000$) are also plotted in Fig. 8 to show the general agreement with the computed results. Note that the computed $S(w')$ increases as the interface is approached and attains a high value of 0.95 there. The high positive skewness means that there was strong (relative to the local rms value) normal motion away from the wall and toward the free surface. This implies that the effect of the upward moving low-momentum fluid ejected near the wall in the event of a burst was felt strongly at the free surface. This interaction between the interface and the burst fluid also occurred in the low-Re flows studied in the experiments of Rashidi and Banerjee.[17] The data of Nakagawa and Nezu do not show a high skewness factor near the interface probably because the effect of the burst was not felt as strongly there; due to the higher Reynolds number in their experiment, the free surface was

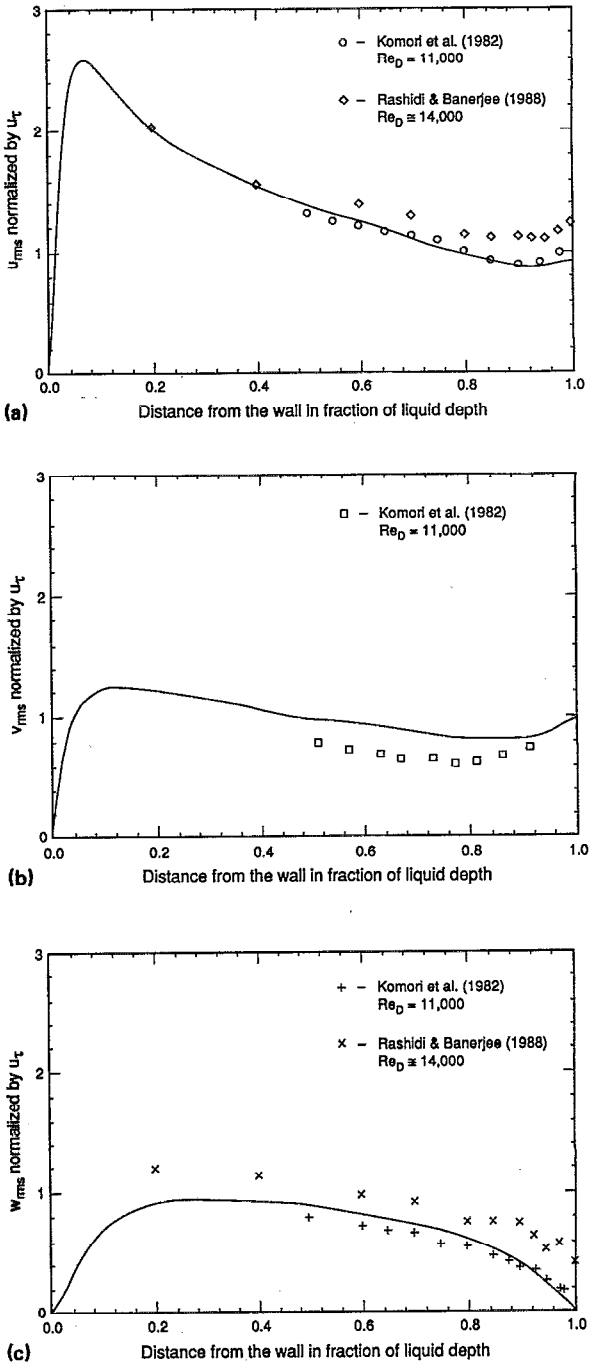

FIG. 7. Comparison between the computed and experimental rms velocity fluctuations near the free surface in case I: (a) u_{rms}, (b) v_{rms}, (c) w_{rms}.

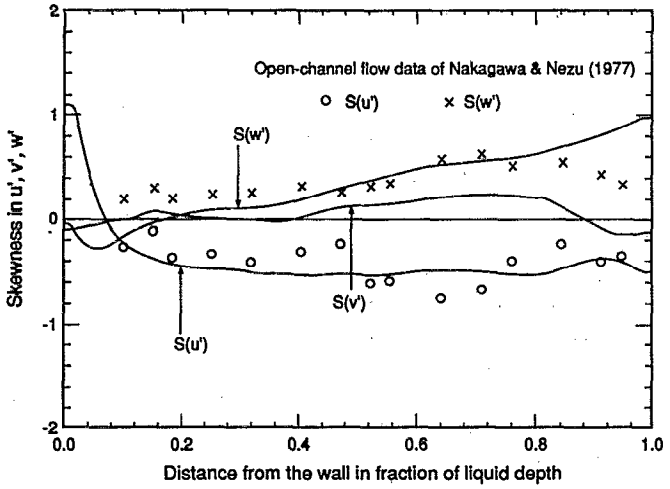

FIG. 8. Comparison between the computed and experimental skewness factors of the velocity fluctuations in case I. $S(u') \equiv \langle u'^3 \rangle / u_{\text{rms}}^{3/2}$, $S(v') \equiv \langle v'^3 \rangle / v_{\text{rms}}^{3/2}$, $S(w') \equiv \langle w'^3 \rangle / w_{\text{rms}}^{3/2}$. The solid lines indicate computed results.

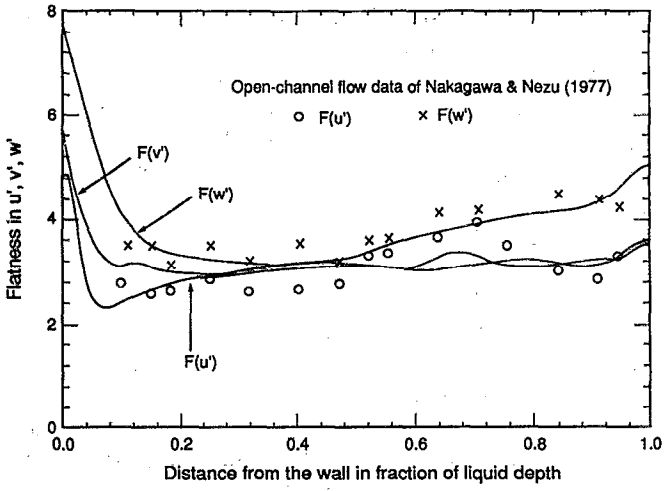

FIG. 9. Comparison between the computed and experimental flatness factors of the velocity fluctuations in case I. $F(u') \equiv \langle u'^4 \rangle / u_{\text{rms}}^2$, $F(v') \equiv \langle v'^4 \rangle / v_{\text{rms}}^2$, $F(w') \equiv \langle w'^4 \rangle / w_{\text{rms}}^2$. The solid lines indicate computed results.

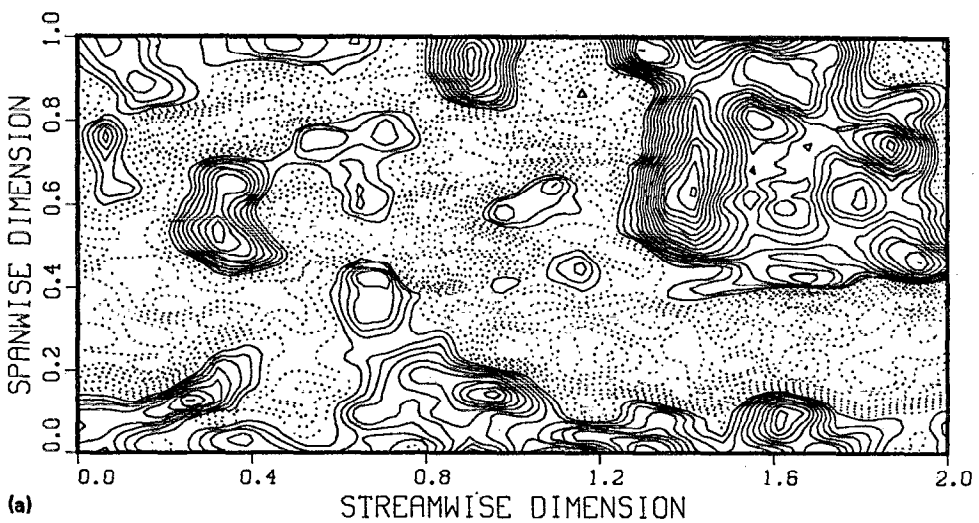

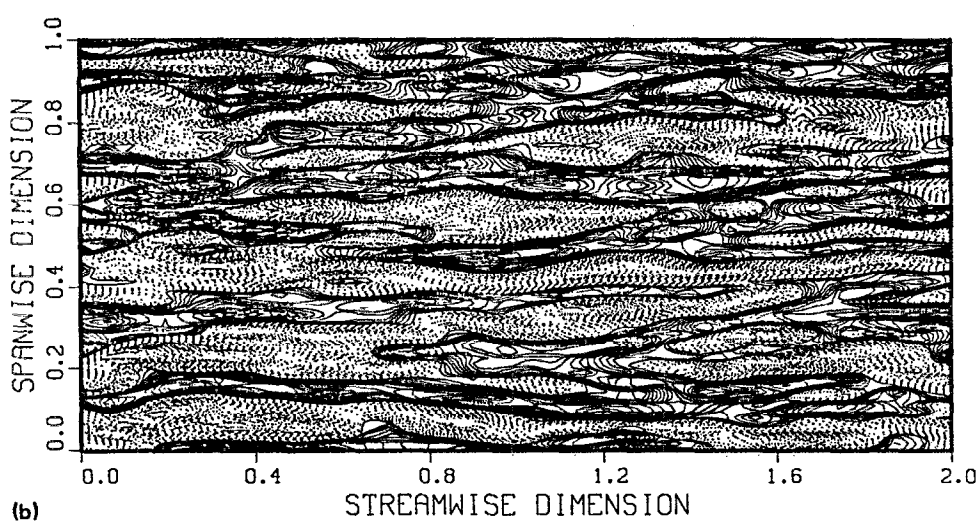

FIG. 10. Contour plots of instantaneous u_1' (case I, $\text{Re}_{*s} = 0$, $\text{Re}_{*w} = 171$) in an x_1-x_2 plane (a) $5\nu/u_{*s}$ from the interface, and (b) $5\nu/u_{*w}$ from the wall. Solid lines represent contours of negative u_1' while dotted lines represent positive contours. The increment between successive contour levels is $0.25u_{*c}$.

farther away (in terms of wall units) from where the burst ejections were produced.

There is also rough agreement between the computed flatness factors and the open-channel flow data of Nakagawa and Nezu,[15] as shown in Fig. 9. Near the wall the computed results also agree generally with the numerical simulation (not shown in Fig. 9) of Kim *et al.*[10] However, at the wall, $F(w')$ is 7.8, rather than ~ 22 as found in Kim *et al.*

B. Streaky structures

To study the low-speed streaks, the computed velocity fields have been used to track particles produced along a line oriented in the spanwise (x_2) direction. This is in effect a simulation of the bubble flow visualization experiments used by, for example, Kline *et al.*,[5] Smith and Metzler,[8] and Rashidi and Banerjee[9] to reveal the low-speed streaks. One major finding of this study is that streaks also form near a free-slip surface (or interface) under shear, in agreement with the experimental observation of Rashidi and Banerjee. Motion pictures have been made of the simulated flow visualization. However, in this paper, the streaky structures are studied by means of the contours of the fluctuating streamwise velocity.

A convenient way to study the streaky structures is provided by the contours of the instantaneous fluctuating streamwise velocity u_1' in a plane parallel to the wall. Some of these contour plots are shown in Figs. 10, 11, and 12 for cases I, V, and VI, respectively. In these plots, solid lines are used to represent contours of negative u_1' and dotted lines for positive u_1'. Because u_1' represents deviation from the mean, the low-speed regions are designated by solid lines in these plots. In agreement with the flow visualization results, the contour plots show that streaks are not found near the interface under no-shear [see Fig. 10(a)]. Going from case I to case VI, the interfacial shear is increased while the wall shear is decreased. By comparing Fig. 10(b) (case I, $\mathrm{Re}_{*w} = 171$) and Fig. 12(b) (case VI, $\mathrm{Re}_{*w} = 53$), we can see that the streaks become more pronounced (as shown by the steeper contours) as the shear is increased near the wall. The same trend can be observed near the free surface by comparing Fig.

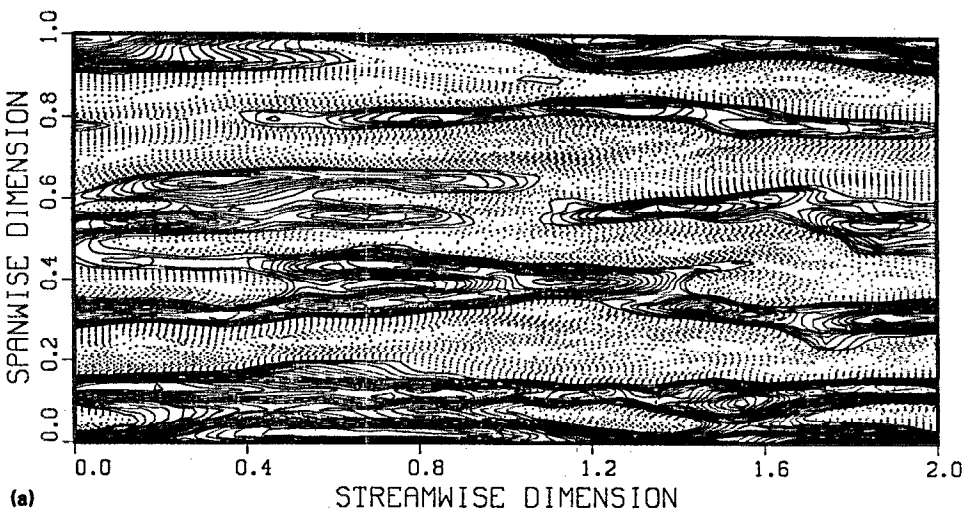

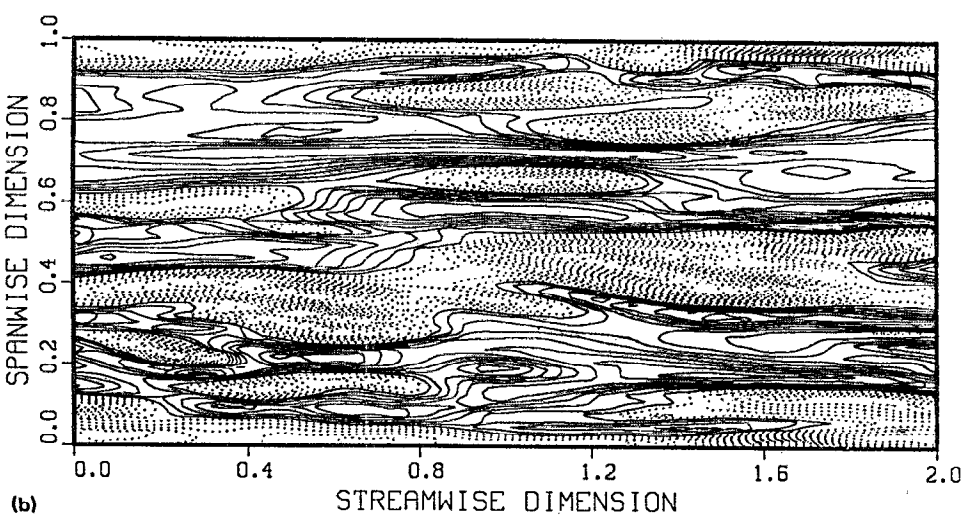

FIG. 11. Contour plots of instantaneous u_1' (case V, $\mathrm{Re}_{*s} = 85$, $\mathrm{Re}_{*w} = 85$) in an x_1-x_2 plane (a) $5\nu/u_{*s}$ from the interface, and (b) $5\nu/u_{*w}$ from the wall. For contour convention see caption of Fig. 10.

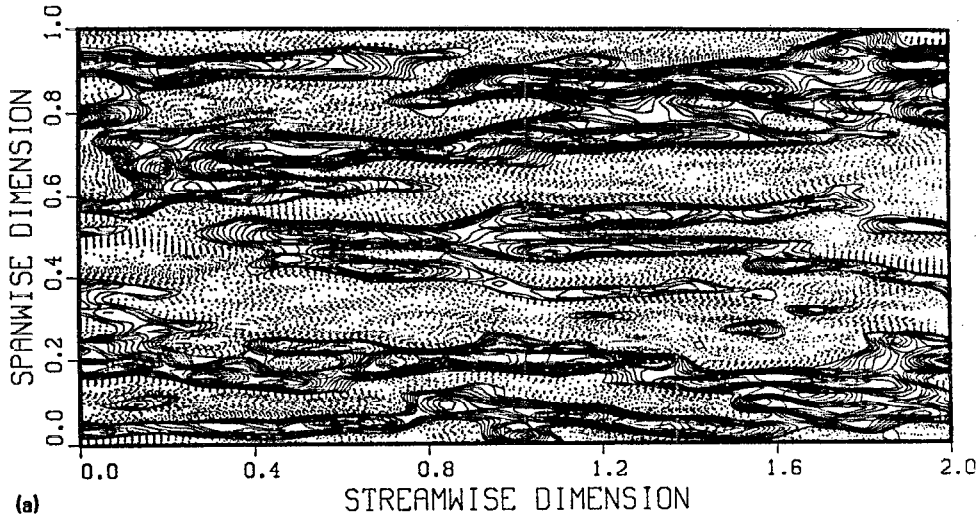

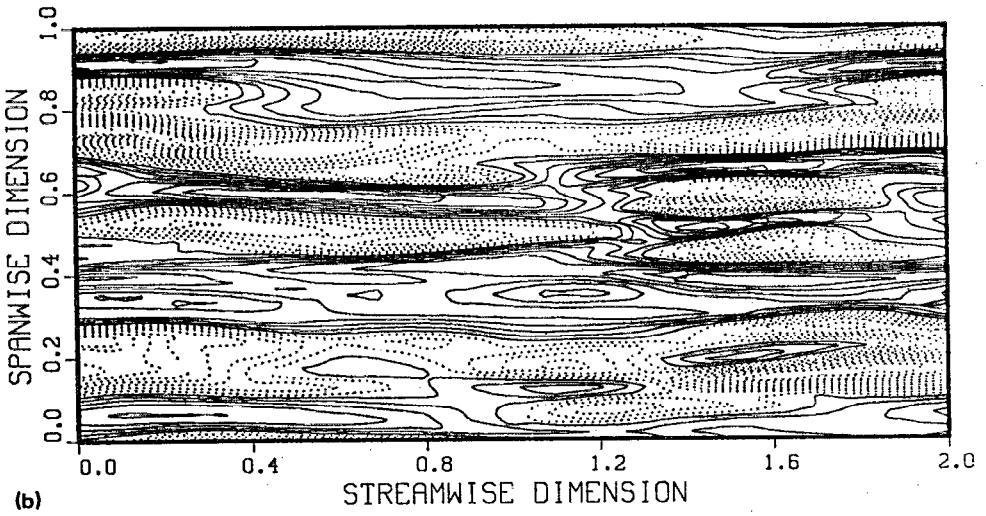

FIG. 12. Contour plots of instantaneous u_1' (case VI, $\mathrm{Re}_{*s} = 122$, $\mathrm{Re}_{*w} = 53$) in an x_1-x_2 plane (a) $5\nu/u_{*s}$ from the interface, and (b) $5\nu/u_{*w}$ from the wall. For contour convention see caption of Fig. 10.

11(a) (case V, $\mathrm{Re}_{*s} = 85$) and Fig. 12(a) (case VI, $\mathrm{Re}_{*s} = 122$).

The average spanwise separation between the streaks has been measured by a method similar to the one used in Smith and Metzler.[8] Figure 13 is a plot of the streak spacing normalized by the appropriate shear velocity ($\lambda_s^+ \equiv \lambda u_{*s}/\nu$ or $\lambda_w^+ \equiv \lambda u_{*w}/\nu$) versus the shear Reynolds number (Re_{*s} or Re_{*w}) for cases I and IV–VI. It can be seen that both λ_s^+ and λ_w^+ fall around 100 in all cases. This result has also been found in the experiments of Rashidi and Banerjee.[9]

After determining that streaks also form near a sheared interface and have much the same characteristics as those found near the wall, the next question to ask is under how much shear do the streaks start to appear. Runs II and III were performed to address that question. As shown in Fig. 14, the small amount of shear imposed at the interface ($\mathrm{Re}_{*s} = 7.6$) in case II is not sufficient to cause streaks. The struc-

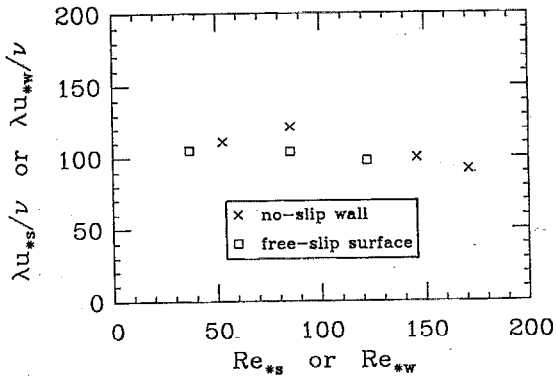

FIG. 13. Normalized mean streak spacing near the wall and free-slip surface at different shear Reynolds numbers. The mean spacing for the wall streaks is normalized by ν/u_{*w} and plotted against Re_{*w}, while that for the free-surface streaks is normalized by ν/u_{*s} and plotted against Re_{*s}.

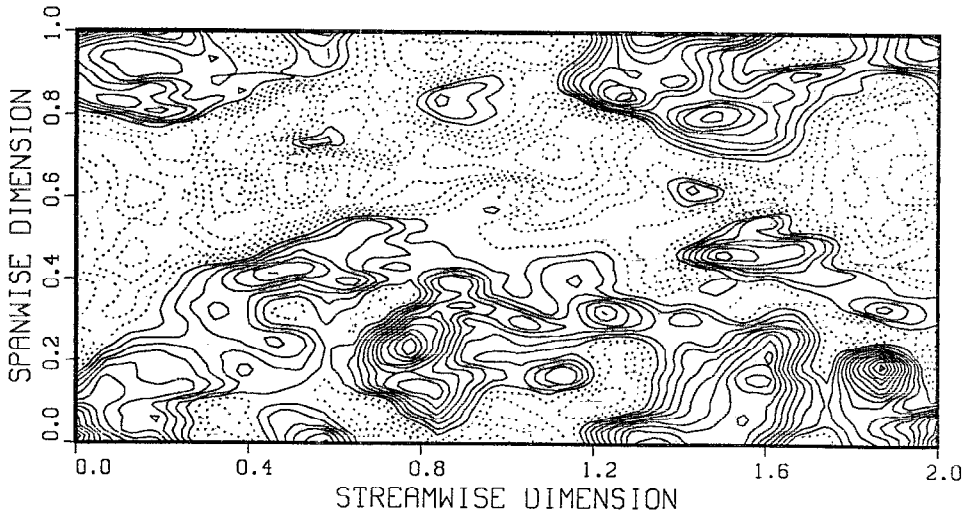

FIG. 14. Contour plots of instantaneous u_1' (case II, $Re_{*s} = 7.6$, $Re_{*w} = 206$) in an x_1-x_2 plane $5\nu/u_{*s}$ from the interface showing no streaky structure. For contour convention see caption of Fig. 10.

tures as Re_{*s} is increased to 26 in case III are shown in Fig. 15. Well-defined streaks are still not seen, but the elongated structure of the streaks formed under higher shear rates becomes noticeable as shown by the high length-to-width ratio of the contour islands. We therefore conclude loosely that $Re_{*s} \simeq 26$ is the critical shear Reynolds number at which streaks start to appear near the interface. We have also looked at what happens near the wall at low shear rates. In case VII, Re_{*w} is reduced to 28 by increasing the shear at the interface. As shown in Fig. 16, the near-wall streaky structures, though still noticeable, appear less well defined. Therefore, $Re_{*w} \simeq 20$ is probably the critical shear Reynolds at which the wall-layer streaks will disappear. In this series of numerical computations, it is not practical to reduce the wall shear further. This is because the interfacial shear will have to be increased to an extent that the steep mean velocity gradient close to the interface cannot be handled accurately with the present numerical resolution. A better simulation to study the effects of low wall shear stress would be to set the wall in motion in the flow direction to reduce the shear stress there. While such experiments have been done (for example, by Uzkan and Reynolds[29] and El Telbany and Reynolds[30,31]), the effect of shear on the wall-layer streaks has not been studied in detail. Uzkan and Reynolds did notice that the streaks disappeared when the velocity of the wall was increased to match with that of the flow. Unfortunately, the condition under which the streaks began to disappear was not discussed.

C. Conditions for the formation of streaks

The significance of the observation of streaks near a free-slip surface is that the presence of a solid wall is not necessary for the generation of the low-speed streaks, confirming the conclusions reached by Lee *et al.*[16] and Rashidi and Banerjee.[9] Therefore, streak formation models which involve a solid boundary will have to be examined with care. For example, the mechanism proposed by Kim[32] for genera-

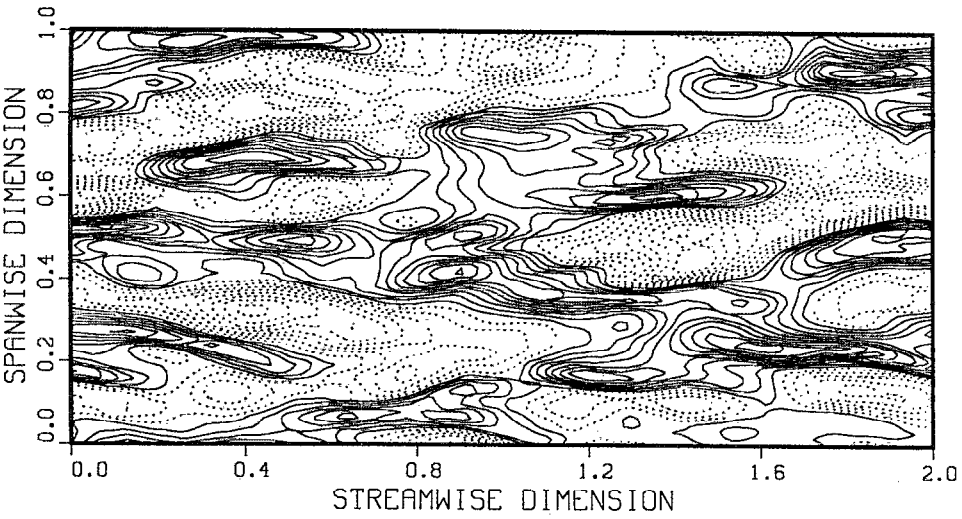

FIG. 15. Contour plots of instantaneous u_1' (case III, $Re_{*s} = 26$, $Re_{*w} = 164$) in an x_1-x_2 plane $5\nu/u_{*s}$ from the interface showing streaky structure beginning to form. For contour convention see caption of Fig. 10.

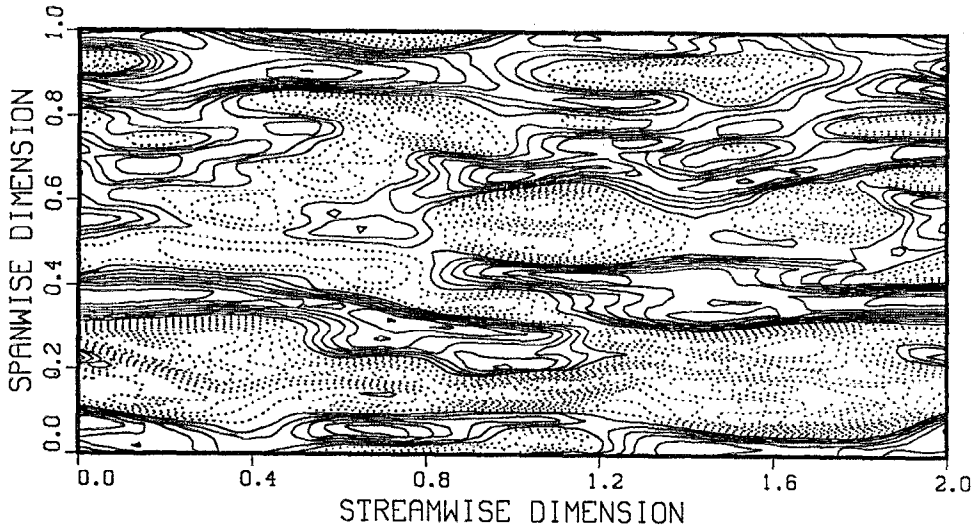

FIG. 16. Contour plots of instantaneous u_1' (case VII, $\mathrm{Re}_{*s} = 168$, $\mathrm{Re}_{*w} = 28$) in an x_1-x_2 plane $5\nu/u_{*w}$ from the wall. For contour convention see caption of Fig. 10.

tion of the counter-rotating streamwise vortices required the no-slip boundary condition on the spanwise velocity component u_2. What we have shown in this study is that streaks also form near a surface when the boundary condition is free-slip, or $\partial u_2/\partial x_3 = 0$.

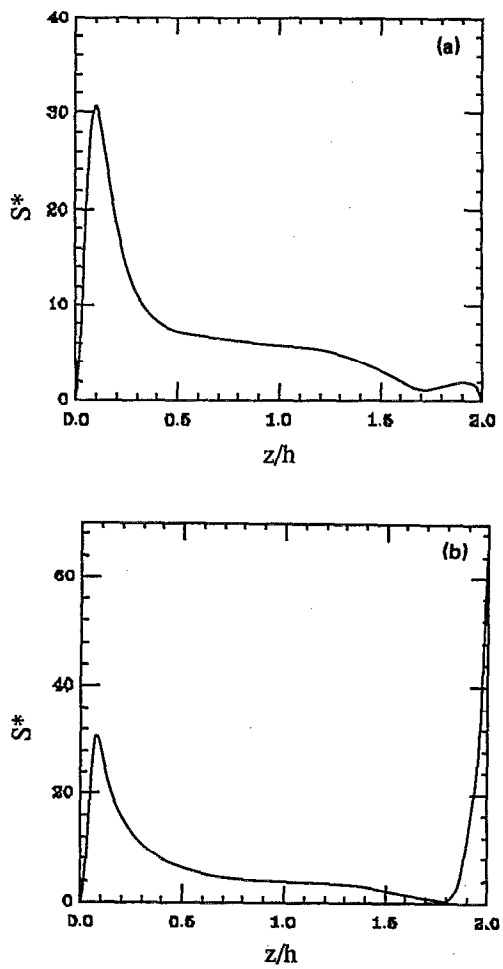

FIG. 17. Profiles of the nondimensional shear rate $S' \equiv Sq^2/\epsilon$ against z/h in (a) case I and (b) case II.

Based on the results discussed in the last section, we see that the shear Reynolds number, Re_{*s} or Re_{*w}, clearly determines whether or not streaks are seen in bounded flows with no-slip and/or free-slip surfaces. However, to understand the *local* conditions required for formation of streaks, it is desirable to seek a parameter that does not depend on the nature of the boundary or on any global variables such as δ_s, δ_w, or h. Lee *et al.*[16] suggested that a candidate for such a parameter is the nondimensional local shear rate

$$S^* \equiv Sq^2/\epsilon, \tag{26}$$

where $S = dU/dz$ is the shear rate, q^2 is twice the turbulent kinetic energy per unit mass, and ϵ is the dissipation rate of $k = \frac{1}{2}q^2$. Their numerical simulations showed that when S^* in a homogeneous flow is ~ 7 (comparable to the value in the outer region of wall-bounded flow), no well-defined streaky structures are seen. However, elongated low-speed streaks become the dominant structures when S^* is increased to 43.2, a value comparable to the maximum $S^* \simeq 37$ that occurs in the wall layer as found in the numerical simulation of Kim *et al.*[10]

We have computed S^* in the different cases we studied to see if it is indeed the parameter which controls streak formation. Figure 17 plots S^* vs z/h for cases I and II. As shown in Fig. 17(a), S^* in case I attains a peak value of 31 in the viscous sublayer (at $z^+ \simeq 8$), drops to ~ 7 farther away from the wall and eventually vanishes at the shear-free interface. This profile agrees quite well with that obtained in the simulation of Kim *et al.* (as shown in Fig. 1 of Lee *et al.*), although there is some discrepancy ($\sim 16\%$) in the peak value. Figure 17(b) shows that in case II, where there is a small shear stress ($\mathrm{Re}_{*s} = 7.6$) at the interface, S^* shoots up to above 60 there. This is because although the shear rate is rather low, $q^2 = u_{\mathrm{rms}}^2 + v_{\mathrm{rms}}^2 + w_{\mathrm{rms}}^2$ remains appreciably finite at the interface because parallel motions are not damped there [see Figs. 7(a) and 7(b)]. Furthermore, the dissipation rate $\epsilon \propto \langle (\partial u_i'/\partial x_j)(\partial u_i'/\partial x_j) \rangle$ is very small at the interface because of the free-slip boundary condition on the parallel velocity fluctuations:

$$\frac{\partial u_1'}{\partial x_3} = \frac{\partial u_2'}{\partial x_3} = 0. \tag{27}$$

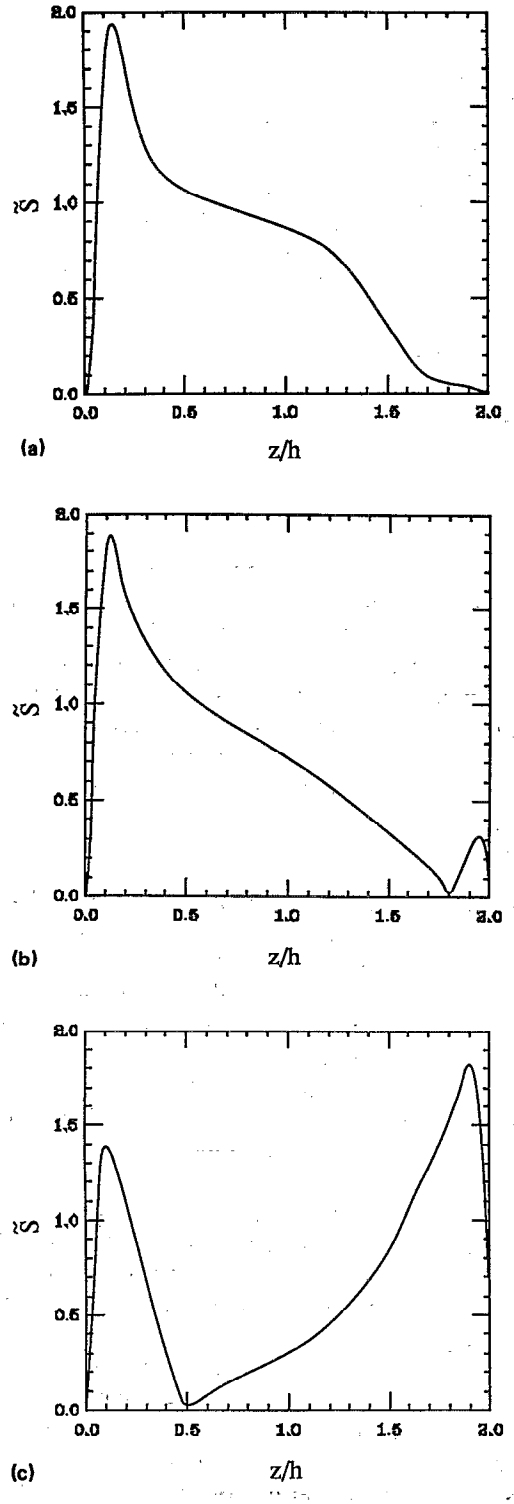

FIG. 18. Profiles of the nondimensional shear parameter $\tilde{S} \equiv S|\langle u'w'\rangle|/\epsilon$ against z/h in (a) case I, (b) case II, and (c) case VII.

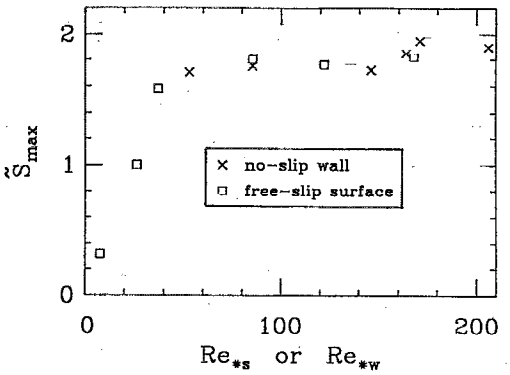

FIG. 19. $\tilde{S}_{max}$ near the interface and the wall against shear Reynolds number, Re_{*w} or Re_{*s}, depending on the corresponding region.

Thus the low value of ϵ combined with the high value of q^2 at the free-slip surface will make S^* rather large, even though the shear rate S itself may be small. Recall that no streaks are seen near the interface in case II. Therefore S^* does not work here as the parameter that controls streak formation. Moreover, it is found that the peak value of S^* near the wall changes little (i.e., stays at ~ 30) even at a rather low wall shear stress, e.g., in case VII where $Re_{*w} = 28$.

To study the condition for streak formation, we consider the shear rate nondimensionalized as

$$S|\langle u'w'\rangle|/\epsilon = \tilde{S}. \tag{28}$$

Figure 18 is a plot of $\tilde{S}$ vs z/h for cases I, II, and VII. In case I, as Fig. 18(a) shows, $\tilde{S}$ has a maximum value of 1.95 close to the wall (at $z^+ \simeq 13$) and decreases to zero at the interface. In case II the near-wall peak value remains roughly the same as in case I but another local maxima of $\tilde{S} \simeq 0.3$ occurs very close to the interface [see Fig. 18(b)]. Figure 18(c) shows that the maximum $\tilde{S}$ near the wall is ~ 1.4 while the maxima near the interface increases to ~ 1.8 in case VII. The variation of the maximum values of $\tilde{S}$ near the wall and near the interface as a function of the shear Reynolds number (Re_{*s} or Re_{*w}) for all the cases studied is plotted in Fig. 19. In general $\tilde{S}_{max}$ is lower at a smaller shear Reynolds number and its value drops faster with Re_{*s} than with Re_{*w}. It can be seen that $\tilde{S}_{max}$ near the interface is 1.0 in case III ($Re_{*s} = 26$), where the interfacial streaks begin to appear. Therefore

$$\tilde{S} \simeq 1.0 \tag{29}$$

may be regarded as the critical nondimensional shear rate which determines formation of the streaks. Although in this study we have not reduced the wall shear rate enough to pinpoint when the streaks begin to disappear it is expected that the above critical condition also applies roughly to the wall-layer streaks.

As can be seen from its definition, Eq. (28), $\tilde{S}$ is the ratio of the rate of production of turbulent kinetic energy ($S|\langle u'w'\rangle|$) to dissipation (ϵ). The streak formation criterion $\tilde{S} \simeq 1.0$ is the condition under which turbulence production balances dissipation. As $\tilde{S} > 1.0$, or production exceeds dissipation, streaks become more evident. However, it is difficult to distinguish the cause and the effect, because it is portions of the low-speed streaks that are ultimately ejected and contribute largely to turbulence production. Looked at from this viewpoint, we have simply found a correlation between the presence of low-speed streaks and turbulence pro-

duction rate exceeding (or equalling) the dissipation rate in a region.

The significance of the nondimensional group $\tilde{S}$ may be considered in another way if we write

$$\tilde{S} = \frac{Sq^2}{\epsilon} \frac{|\langle u'w' \rangle|}{q^2} = S^* \frac{|\langle u'w' \rangle|}{q^2}. \tag{30}$$

The group $|\langle u'w' \rangle|/q^2$ represents the ratio of the shear to the normal (diagonal) components of the turbulent stresses. It is a measure of the degree of anisotropy of the turbulent motions. Here S^* can be thought of as the ratio between two time scales:

$$S^* = t_T/t_S, \tag{31}$$

where $t_S = 1/S$ is the time scale of deformation caused by the mean shear rate and t_T represents the turbulent time scale given by the turbulent length scale q^3/ϵ divided by the turbulent velocity scale q. Therefore $\tilde{S}$ combines the effects of anisotropy and of the rate of deformation of the fluid imposed by the mean shear rate. The critical condition expressed in $\tilde{S}$ means that for streaks to occur, we must have a sufficiently rapid mean deformation (compared to turbulent fluctuations) and/or significant shear component of the turbulent stresses.

IV. SUMMARY AND CONCLUSIONS

We have performed a series of numerical simulations of a flow between a wall and a free-slip surface in which different shear rates can be applied at both surfaces. In agreement with the recent experiment of Rashidi and Banerjee (1990), the present results show that the low-speed streaks that have been observed near walls in many previous studies also occur near the free-slip surface (or gas–liquid interface) under a sufficiently high shear rate. The streaks found near the free surface, although appearing somewhat more pronounced, have similar characteristics as the wall-layer streaks. For example, streaks occurring near both surfaces have the same mean spanwise spacing of ~ 100 when normalized by ν and the appropriate shear velocity, u_{*w} or u_{*s}. We therefore conclude that the nature of the boundary is much less important than the shear rate in determining formation of the streaks. As mentioned earlier we did not expect such a result since vortex lines can attach at a free-slip boundary and a wall-normal component of vorticity can exist. Considering that many of the turbulence phenomena at no-slip boundaries appear to be associated with quasistreamwise vortices and their interactions with low-speed streaks, it was surprising that such strong similarities exist with a situation where vortices with wall-normal axes can attach, viz., a free-slip boundary.

The dependence of the streaky structures on shear rate can be expressed in terms of the local shear parameter $\tilde{S} \equiv S|\langle u'w' \rangle|/\epsilon$. In the present study, the condition for streaks to appear is found to be $\tilde{S} > \sim 1.0$. Physically, this condition suggests that a sufficiently rapid mean deformation (compared to the turbulent fluctuations) and/or a significant shear component of the turbulent stresses are required for streaks to occur.

ACKNOWLEDGMENTS

The computations were done on the Cray XMP/48's at the San Diego Supercomputer Center and at NCSA, University of Illinois, Urbana—Champaign.

This work has been supported by the U.S. Department of Energy, Office of Energy Research, under Contract No. DE-FG03-85ER13314.

[1] A. Fage and H. C. H. Townend, "An examination of turbulent flow with an ultramicroscope," Proc. R. Soc. London Ser. A **135**, 656 (1932).

[2] J. K. Ferrell, F. M. Richardson, and K. O. Beatty, "Dye displacement technique for velocity distribution measurement," Ind. Eng. Chem. **47**, 29 (1955).

[3] F. R. Hama, J. D. Long, and J. C. Hegarty, "On transition from laminar to turbulent flow," J. Appl. Phys. **28**, 388 (1957).

[4] F. A. Schraub and S. J. Kline, "A study of the structure of turbulent boundary layer with and without longitudinal pressure gradients," Department of Mechanical Engineering Report No. MD-12, Stanford University, 1965.

[5] S. J. Kline, W. C. Reynolds, F. A. Schraub, and P. W. Runstadler, "The structure of turbulent boundary layers," J. Fluid Mech. **30**, 741 (1967).

[6] R. F. Blackwelder and H. Eckelmann, "Streamwise vortices associated with the bursting phenomenon," J. Fluid Mech. **94**, 577 (1979).

[7] H. Nakagawa and I. Nezu, "Structure of space-time correlation of bursting phenomena in an open channel flow," J. Fluid Mech. **104**, 1 (1981).

[8] C. R. Smith and S. P. Metzler, "The characteristics of low-speed streaks in the near-wall region of a turbulent boundary layer," J. Fluid Mech. **129**, 27 (1983).

[9] M. Rashidi and S. Banerjee, "The effect of boundary conditions and shear rate on streak formation and breakdown in turbulent channel flows," Phys. Fluids A **2**, 1827 (1990).

[10] J. Kim, P. Moin, and R. Moser, "Turbulence statistics in fully developed channel flow at a low Reynolds number," J. Fluid Mech. **177**, 133 (1987).

[11] K. Lam and S. Banerjee, "Investigation of turbulent flow bounded by a wall and a free surface," in *Fundamentals of Gas–Liquid Flows*, edited by E. E. Michaelides and M. P. Sharma (ASME, New York, 1988), Vol. 72, pp. 29–38.

[12] H. T. Kim, S. J. Kline, and W. C. Reynolds, "The production of turbulence near a smooth wall in a turbulent boundary layer," J. Fluid Mech. **50**, 133 (1971).

[13] R. S. Brodkey, J. M. Wallace, and H. Eckelmann, "Some properties of truncated turbulence signals in bounded shear flows," J. Fluid Mech. **63**, 1209 (1974).

[14] W. W. Willmarth, "Structure of turbulence in boundary layers," *Advances in Applied Mechanics* (Academic, New York, 1975), Vol. 15, pp. 159–254.

[15] H. Nakagawa and I. Nezu, "Prediction of the contributions to the Reynolds stress from the bursting events in open channel flows," J. Fluid Mech. **80**, 99 (1977).

[16] M. J. Lee, J. Kim, and P. Moin, "Turbulence structure at high shear rate," in Proceedings of the Sixth Symposium on Turbulent Shear Flows, Toulouse, France, 7–9 September 1987.

[17] M. Rashidi and S. Banerjee, "Turbulence structure in free surface channel flows," Phys. Fluids **31**, 2491 (1988).

[18] T. Gerz, U. Schumann, and S. E. Elghobashi, "Direct numerical simulation of stratified homogeneous turbulent shear flows," J. Fluid Mech. **200**, 563 (1989).

[19] M. M. Rogers and P. Moin, "The structure of the vorticity field in homogeneous turbulent flows," J. Fluid Mech. **176**, 33 (1987).

[20] J. J. Riley, R. W. Metcalfe, and S. A. Orszag, "Direct numerical simulations of chemically reacting turbulent mixing layers," Phys. Fluids **29**, 241 (1986).

[21] U. Schumann, G. Grotzbach, and L. Kleiser, "Direct numerical simulation of turbulence," in *Prediction Methods for Turbulent Flows*, edited by W. Kollman (Hemisphere, New York, 1980), p. 123.

[22] R. S. Rogallo and P. Moin, "Numerical simulation of turbulent flows," Annu. Rev. Fluid Mech. **16**, 99 (1984).

[23] K. Lam, "Numerical simulation of turbulent flow bounded by a wall and a free-slip surface," Ph.D. thesis, University of California at Santa Barbara, 1989.

[24]H. Kreplin and H. Eckelmann, "Behavior of the three fluctuating velocity components in the wall region of a turbulent channel flow," Phys. Fluids **22**, 1233 (1979).
[25]S. Komori, H. Ueda, F. Ogino, and T. Mizushima, "Turbulence structure and transport mechanism at the free surface in an open channel flow," Int. J. Heat Mass Transfer **25**, 513 (1982).
[26]G. Comte-Bellot, "Contribution a l'étude de la turbulence de conduite," Doctoral thesis, University of Grenoble, France, 1963.
[27]P. Moin and J. Kim, "Numerical investigation of turbulent channel flow," J. Fluid Mech. **118**, 341 (1982).
[28]I. Nezu and W. Rodi, "Open-channel flow measurements with a laser Doppler anemometer," J. Hydraul. Eng. **112**, 335 (1986).
[29]T. Uzkan and W. C. Reynolds, "A shear-free turbulent boundary layer," J. Fluid Mech. **28**, 803 (1967).
[30]M. M. M. El Telbany and W. C. Reynolds, "Velocity distributions in plane turbulent channel flows," J. Fluid Mech. **100**, 1 (1980).
[31]M. M. M. El Telbany and W. C. Reynolds, "Turbulence in plane channel flows," J. Fluid Mech. **111**, 283 (1981).
[32]J. Kim, "On the structure of wall-bounded turbulent flows," Phys. Fluids **26**, 2088 (1983).